

# High confinement micron-scale silicon nitride high Q ring resonator

Alexander Gondarenko<sup>1</sup>, Jacob S. Levy<sup>2</sup> and Michal Lipson<sup>2</sup>

1. School of Applied and Engineering Physics, Cornell University, Ithaca, NY, 14853.

2. School of Electrical and Computer Engineering, Cornell University, Ithaca, NY, 14853.  
[aag42@cornell.edu](mailto:aag42@cornell.edu)

**Abstract:** We demonstrate high confinement, low-loss silicon nitride ring resonators with intrinsic quality factor ( $Q$ ) of  $3 \times 10^6$  operating in the telecommunication C-band. We measure the scattering and absorption losses to be below 0.065dB/cm and 0.055dB/cm, respectively.

© 2009 Optical Society of America

**OCIS codes:** (140.3945) Microcavities; (130.3130) Integrated optics devices; (130.3130) Integrated optics materials

---

## References and links

1. K. Ikeda, R. E. Saperstein, N. Alic, and Y. Fainman, "Thermal and Kerr nonlinear properties of plasma-deposited silicon nitride/ silicon dioxide waveguides," *Opt. Express* **16**(17), 12987–12994 (2008).
2. J. N. Milgram, J. Wojcik, P. Mascher, and A. P. Knights, "Optically pumped Si nanocrystal emitter integrated with low loss silicon nitride waveguides," *Opt. Express* **15**(22), 14679–14688 (2007).
3. S. Gaugiran, S. Gétin, J. Fedeli, G. Colas, A. Fuchs, F. Chatelain, and J. Dérourard, "Optical manipulation of microparticles and cells on silicon nitride waveguides," *Opt. Express* **13**(18), 6956–6963 (2005).
4. A. Serpengüzel, "Amorphous silicon nitride microcavities," *J. Opt. Soc. Am. B* **18**(7), 989–993 (2001).
5. N. Daldosso, M. Melchiorri, F. Riboli, F. Sbrana, L. Pavesi, G. Pucker, C. Kompocholis, M. Crivellari, P. Bellutti, and A. Lui, "Fabrication and optical characterization of thin two-dimensional Si<sub>3</sub>N<sub>4</sub> waveguides," *Mater. Sci. Semicond. Process.* **7**(4-6), 453–458 (2004).
6. C. A. Barrios, B. Sánchez, K. B. Gylfason, A. Griol, H. Sohlström, M. Holgado, and R. Casquel, "Demonstration of slot-waveguide structures on silicon nitride / silicon oxide platform," *Opt. Express* **15**(11), 6846–6856 (2007).
7. K. Foubert, L. Lalouat, B. Cluzel, E. Picard, D. Peyrade, E. Delamadeleine, F. de Fornel, and E. Hadji, "Near-field modal microscopy of subwavelength light confinement in multimode silicon slot waveguides," *Appl. Phys. Lett.* **93**(25), 251103 (2008).
8. L. Vivien, D. Marris-Morini, A. Griol, K. B. Gylfason, D. Hill, J. Alvarez, H. Sohlström, J. Hurtado, D. Bouville, and E. Cassan, "Vertical multiple-slot waveguide ring resonators in silicon nitride," *Opt. Express* **16**(22), 17237–17242 (2008).
9. M. Shaw, J. Guo, A. Vawter, S. Habermehl, and C. Sullivan, "Fabrication techniques for low loss silicon nitride waveguides," *Proc. SPIE* **5720**, 109 (2005).
10. J. Guo, M. J. Shaw, G. A. Vawter, P. Esherrick, G. R. Hadley, and C. T. Sullivan, "High-Q integrated on-chip micro-ring resonator," in *Proc. 17th Annu. Meeting IEEE/LEOS*, **2**, pp. 745, (2004).
11. E. Shah Hosseini, S. Yegnanarayanan, M. Soltani, and A. Adibi, "Ultra-High Quality Factor Microdisk Resonators for Chip-Scale Visible Integrated Photonics," in *Frontiers in Optics*, FMG4 (2008).
12. A. Gorin, A. Jaouad, E. Grondin, V. Aimez, and P. Charette, "Fabrication of silicon nitride waveguides for visible-light using PECVD: a study of the effect of plasma frequency on optical properties," *Opt. Express* **16**(18), 13509–13516 (2008).
13. V. R. Almeida, R. R. Panepucci, and M. Lipson, "Nanotaper for compact mode conversion," *Opt. Lett.* **28**(15), 1302–1304 (2003).
14. M. Borselli, T. J. Johnson, and O. Painter, "Accurate measurement of scattering and absorption loss in microphotonic devices," *Opt. Lett.* **32**(20), 2954–2956 (2007).
15. P. Barclay, K. Srinivasan, and O. Painter, "Nonlinear response of silicon photonic crystal microresonators excited via an integrated waveguide and fiber taper," *Opt. Express* **13**(3), 801–820 (2005).

---

Silicon nitride (Si<sub>3</sub>N<sub>4</sub>) is a promising material for a waveguide platform due to its low nonlinearity [1] and its transparency in both the visible and infrared spectrum [2–4]. To date silicon nitride waveguides have not been widely employed for propagation at the infrared due to the high tensile stress which limits the thickness of low pressure chemical vapor deposited (LPCVD) Si<sub>3</sub>N<sub>4</sub> films to around 250 nm [5–8]. The small film thickness limits the lowest loss modes to quasi-TE (electric field polarized in the substrate plane) which are poorly confined in the nitride and have a very small effective mode index ( $n_{eff}$ ) < 1.6. Highly delocalized waveguides in the C-band have demonstrated losses as low as 0.1 dB/cm [9] and rings, with diameters as large as several mm, have been shown with quality factors as high as  $2.4 \times 10^5$  [10]. In the visible spectrum, Adibi *et al.* demonstrated structures with  $Q$ 's over  $4 \times 10^6$  at

wavelength of 655 nm [11]. Plasma enhanced chemical vapor deposition (PECVD) has been recently optimized to deposit  $\text{Si}_x\text{N}_y$  nitride films at low temperature (400°C) with losses below 1 dB/cm at wavelength of 532nm [12].

We demonstrate a method based on temperature cycling and annealing for fabricating low loss  $\text{Si}_3\text{N}_4$  waveguides with highly confined optical modes. We achieve losses down to 0.12 dB/cm and intrinsic  $Q$ 's up to 3,000,000 in single mode ring resonators (Fig. 1). We successfully deposited films up to 744nm in thickness. This thickness, sufficient for the high confinement waveguides used here does not appear to be an absolute limit. A single mode waveguide at this thickness is strongly confined, with an effective index reaching  $\sim 1.75$  for both TE and TM (compared to the bulk material index  $\sim 2.0$ ).

We fabricate our devices on thermally oxidized silicon wafers. Stoichiometric silicon nitride is deposited in an LPCVD oven at 800°C and 0.1 mTorr. To deposit thick films we cycle the temperature in the deposition process. Layers over 400 nm thick are deposited in multiple steps, allowing wafers to cool to room temperature in between depositions. MaN 2403 e-beam resist is used for patterning with a JEOL 9300 E-beam system. We use a post exposure bake for 5 minutes at 145°C to reflow the resist surface and reduce sidewall roughness. During the reflow the top surface of resist shrinks by  $\sim 1$ -10% depending on the resist thickness while the bottom surface remains attached to the nitride and does not change size. An inductively coupled plasma reactive ion etcher (ICP RIE), Oxford 100, is used to etch the devices with a  $\text{CHF}_3/\text{O}_2$  chemistry. Note that etching a 4" wafer with a thickness greater than 400nm requires a pause of the etching process, and the etching of the nitride from the back of the wafer in order to ensure that the thick nitride layer on the backside does not cause excessive stress and break the wafer. Devices are annealed at 1200°C for 20 min in oxygen atmosphere at 1 atm and then in a nitrogen atmosphere for 3 hours. Annealed devices are clad with 460 nm of high temperature silicon dioxide (HTO) deposited at 800°C at 0.2 mTorr. A final silicon dioxide cladding was deposited using a PECVD tool.

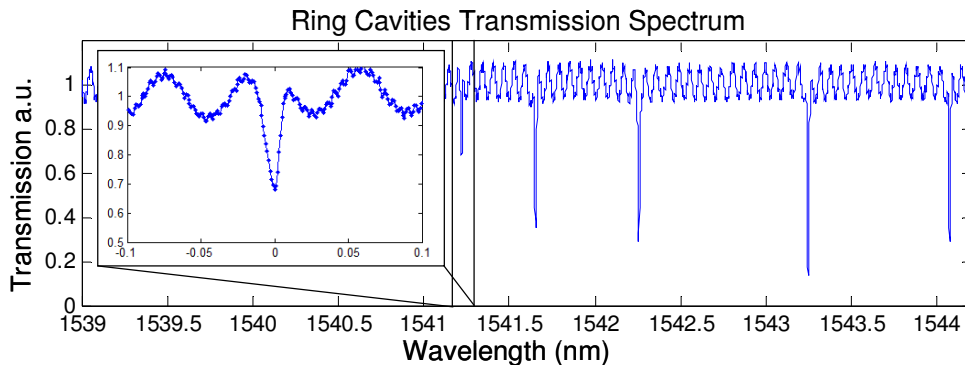


Fig. 1. Transmission spectrum of multiple 40  $\mu\text{m}$  diameter rings coupled to a waveguide. Inset, high resolution spectrum of a  $1.5 \times 10^6$  coupled Q ring,  $5.4 \times 10^6$  intrinsic Q, 0.065 dB/cm loss in ring.

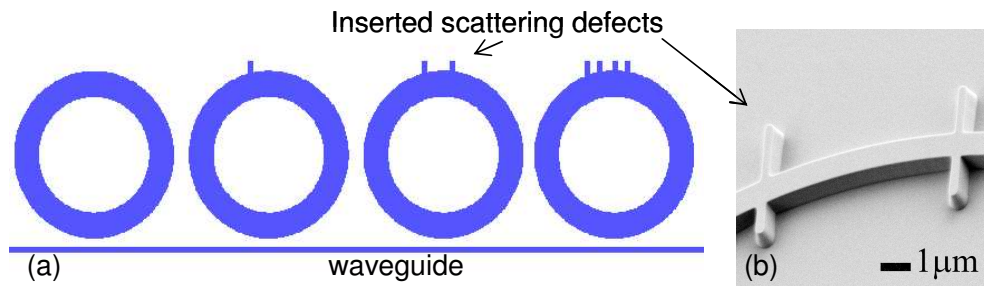


Fig. 2. (a) A series of ring resonators coupled to a single waveguide. The resonators have slightly different radii to distinguish their transmission spectra. (b) SEM micrograph of scattering defects (vertical bars) across a ring resonator inserted to separately measure scattering and absorption losses.

We fabricate multiple ring resonators with radii of  $\sim 20$   $\mu\text{m}$ , height 644 nm, and width of 900 nm coupled to a bus waveguide of the same dimensions. The devices are clad on top and bottom with 4 microns of silicon dioxide. The circumferences of each ring in the series of resonators varies by 80nm to distinguish their resonances. Each ring has from 0 to 8 defects introduced, Fig. 2(b), to increase scattering losses and reduce the  $Q$ . The waveguides were terminated with tapers to improve coupling light to fiber [13]. The difference between TE and TM effective indices was  $\sim 0.03$  and minor field component in both polarizations was  $< 10\%$  of the major field component. The rectangular cross section was chosen to minimize coupling between the polarizations. The measurement of transmission spectrum of the waveguide coupled rings showed distinct TE and TM resonances with high ( $> 20\text{dB}$ ) extinction for both, ensuring polarization stability.

In order to accurately distinguish between scattering and absorption losses, we introduce carefully engineered defects in the cavities and use Borselli's method [14] to extract linear absorption and scattering coefficients from the optical cavity spectrum. The method consists of measuring the shift of the cavity resonance as a function of the input power coupled into the ring, Fig. 3. The red shift is caused by the temperature increase in the cavity. The temperature change is only dependent on the absorption coefficient (and not on the scattering). The resonance shift as a function of the input power is measured for several rings with different intrinsic quality factors to accurately calculate contributions from different loss mechanisms. The quality factor determines the degree of built up energy in the ring, and therefore the dependence of the resonance shift with the input power.

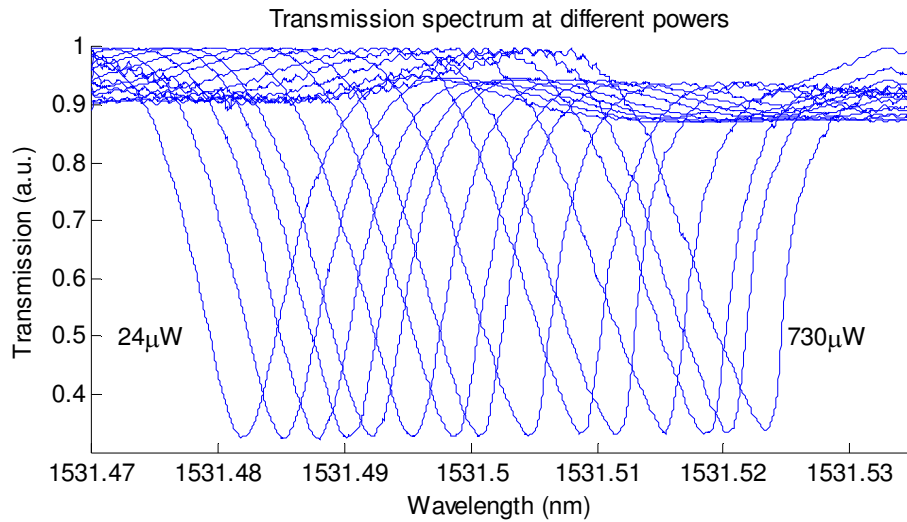


Fig. 3. Shift in the transmission spectra of a waveguide coupled ring with increasing coupled power. Input laser power heats the ring, causing an increase in the refractive index and in turn shifts in the resonance spectrum. The laser power is not sufficient to cause nonlinear absorption hence the  $Q$  of the ring does not change, as is evident by the constant extinction ratio across all coupled powers.

We measure the  $Q$  of rings with different number of artificial defects and from the difference between  $Q$ 's find that each scatterer contributes  $0.15 \pm 0.05$  dB/cm of attenuation in the ring. Figure 3 shows the red shift of the resonances for one of the rings without defects. The slight asymmetry of the resonance at high input power is due to the bistability, typical of high  $Q$  rings. Figure 4 shows the extracted resonance shift from plots such as Fig. 3 for rings with different number of defects. The resonance shift shows strong linear dependence on the coupled power indicating low nonlinearities (Fig. 4). Quadratic fit of resonance shift to power dropped indicates nonlinear losses were 2% of total losses in the cavity. We measure coupled  $Q$  for a ring without scatterers to be 244,000 with 70% transmission on resonance corresponding to intrinsic  $Q$  of 3,000,000 [15] and an intrinsic attenuation coefficient of 0.12 dB/cm.

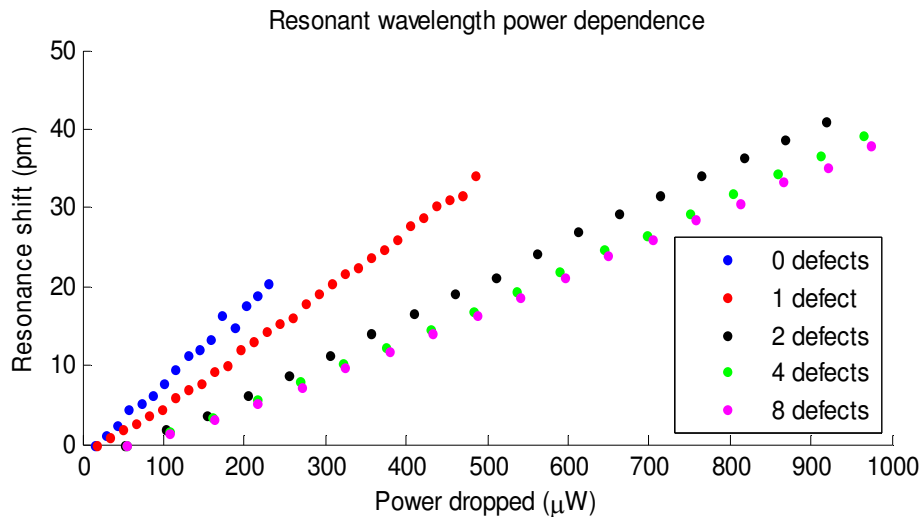


Fig. 4. Shift of ring resonance at different coupled power. Rings with scattering defects absorb less of the coupled power and hence have small resonance shift.

We estimate the scattering and absorption losses to be below 0.065dB/cm and 0.055dB/cm, respectively. These losses are extracted from the resonance shift dependence on the power dropped by the ring,  $P_d$ , given by  $\Delta\lambda(P_d) = C(\gamma_a / \gamma_t)P_d$ , where  $C$  is the thermal coefficient of the effective index of the waveguide,  $(\gamma_a / \gamma_t)P_d$  is the fraction of dropped power absorbed by the material in the cavity,  $\gamma_a$  is the absorption loss coefficient, and  $\gamma_t$  is the total loss coefficient in the cavity. The total loss coefficient is the sum of all losses  $\gamma_t = \gamma_e + \gamma_a + \gamma_s$ , where  $\gamma_s$ , is the loss due to scattering and  $\gamma_e$  is the unloading loss from the ring to the bus waveguide calculated from the measured low power transmission lorentzian line shape [14,15]. The shift over power ratio  $\Delta\lambda(P_d) / P_d = C(\gamma_a / \gamma_t) = S$  is extracted from Fig. 4 for the different rings. The thermal coefficient  $C = 0.01 \text{ pm}/\mu\text{W}$  is extracted from resonance shifts nonlinear dependence on dropped power by fitting a quadratic dependence of resonance shift on  $P_d$ . The absorption loss coefficient,  $\gamma_a$ , is then found by extracting  $\gamma_t$  for each ring.

The demonstrated silicon nitride devices in this work have the lowest loss and highest confinement to our knowledge in the near infrared spectrum. We achieve low losses utilizing resist reflow, temperature cycled deposition, and etch optimization in our process flow. The temperature cycling allows us to overcome the nitride stress limit and deposit thick films, enabling the fabrication of high confinement waveguides. The low loss and high confinement are applicable for low power, dense on chip integration.

### Acknowledgements

The authors gratefully acknowledge support from the Devices for Information Technology Research (CMDITR) - University of Washington and National Science Foundation Center on Materials as well as support from the DARPA MTO POPS Program.